Defects in Strontium Titanate: A First Principles Study

Mina Bahrami*, Dominic Waldhoer*, Pedram Khakbaz*, Theresia Knobloch*,
Aftab Nazir†, Changze Liu†, and Tibor Grasser*
* Institute for Microelectronics, Technische Universität Wien, Gußhausstraße 27–29, 1040 Vienna, Austria
† Huawei Technologies R&D Belgium NV
Email: bahrami | grasser@iue.tuwien.ac.at

***Abstract*—In recent years there has been growing interest in exploring new 2D material-based devices with improved scalability. For achieving good device performance, the need for choosing appropriate dielectrics has become evident. One promising candidate is Strontium Titanate, $SrTiO_3$, which is a high-κ perovskite that can be transferred on 2D MoS_2 and WSe_2 to fabricate high-performance n- and p-type FETs. In this work we use density functional theory in conjunction with a hybrid functional to study the potential relevance of four different kinds of intrinsic defects in $SrTiO_3$ for device performance and reliability. The defect parameters describing charge trapping are obtained using non-radiative multiphonon theory which can then be used in future TCAD and compact modeling studies. We show that based on its trap level, the titanium antisite defect is a relevant defect for MoS_2/$SrTiO_3$ based devices.**

***Index Terms*—$SrTiO_3$, defects, 2D materials, reliability, non-radiative multiphonon (NMP) theory**

I. INTRODUCTION

Two-dimensional materials such as transition metal dichalcogenides (TMDs) offer high mobility, atomically thin device channels and relatively defect-free layers, which renders them a very promising material system for the channel in next-generation ultrascaled field-effect transistors (FETs) [1]. However, the use of 2D materials in nanoelectronic devices faces a considerable challenge, namely the lack of high-k dielectrics with atomically sharp and flat interfaces [2,3]. In this context, $SrTiO_3$ has recently been proposed as a potentially suitable gate dielectric for 2D material-based FETs [4,5]. However, in order to ensure stable and reliable operation of e.g. molybdenum disulfide (MoS_2) FETs using $SrTiO_3$ (STO) as a gate insulator, it is important to understand the prevalent point defects in this material [6,7]. The structural and electronic properties of materials are considerably influenced by defects. Perovskites and amorphous oxides, in particular, possess a significant number of native defects due to their structural complexity and possible deviations from stoichiometry. As a result, the properties of these oxides are primarily determined by the type and quantity of defects present in their lattices. Insulator defects are suspected to be responsible for the hysteresis, bias temperature instabilities (BTI) [8] and random telegraph noise (RTN) [9] in metal oxide semiconductor field effect transistor (MOSFET) devices because they can capture charges from the substrate during operation. These mechanisms involve charge transitions and can be described by a non-radiative multiphonon (NMP) process [10,11].

Here, we use density functional theory (DFT), employing a hybrid functional to determine crucial defect parameters such as the relaxation and formation energies as well as thermodynamic trap levels. These are the essential input parameters for physical charge trapping models based on NMP theory, enabling the prediction of degradation over the course of the device lifespan [7].

II. NMP MODEL FOR CHARGE TRAPPING

The transfer of charge between a defect in the dielectric and the 2D semiconductor is governed by NMP transitions [12]. Within the NMP model the two interacting charge states, named 1 and 2, are treated as coupled quantum mechanical harmonic oscillators [11]. Typically, to create an efficient and concise model for characterizing charge transitions during a TCAD simulation, various approximations are utilized. For instance, the vibrational motion is assumed to take place along a single effective mode, resulting in a so-called reaction coordinate. In this approximation, the two defect states are described by two parabolic potential energy curves (PEC) as illustrated in Fig. 1.

III. FIRST-PRINCIPLE CALCULATIONS

All calculations were performed on a $4 \times 4 \times 4$ cubic cell of $SrTiO_3$ using the Gaussian Plane Wave

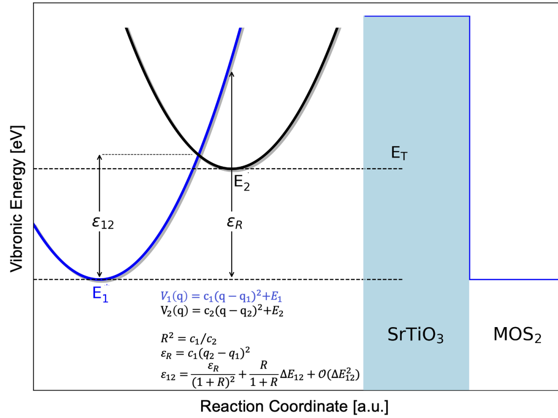

Figure 1: Schematics of charge transfer within the NMP model. The transfer of charges is modelled by two 1D harmonic oscillators which interact due to electron-phonon coupling. Their potential energy curves are parameterized by the relaxation energy $\mathcal{E}_{\mathrm{R}}$ and the trap level $\mathrm{E_T}$.

(GPW) method with the double-ζ Gaussian basis set being employed in combination with the Goedecker-Teter-Hutter (GTH) pseudopotentials [13] as implemented in the CP2K code [14], with an energy cutoff of 700 Ry. To minimize the errors of electronic state calculations we used the PBE0-TC-LRC hybrid functional for all the calculations and a mixing factor $\alpha = 0.25$ for the Hartree-Fock(HF) exchange. The Broyden-Fletcher-Goldfarb-Shanno (BFGS) algorithm was used to perform geometry optimizations in different charge states. We independently compared our simulation results to experimental data for a variety of well-known properties of bulk $SrTiO_3$ to verify the accuracy of our simulation setup as summarized in Tab. I. Our calculations show good agreement for the lattice constants, static and optical permittivities, indicating their suitability for describing the material. The permittivities were evaluated by the change in polarization after applying a finite electric field using the Berry phase formalism [15].

		PBE0 (α=0.25)	Exp.	[ref.]
Lattice Constant a	[Å]	3.94	3.90	[16]
Indirect Bandgap E_{G}	[eV]	3.30	3.25	[17]
Optical Permittivity ϵ_∞	[1]	4.31	4.64	[18]
Static Permittivity ϵ_0	[1]	214	300	[19]

Table I: Comparison of cubic $SrTiO_3$ bulk properties calculated by our DFT setup compared to experimental data.

Initial defect configurations were created manually within the structure followed by a geometry optimization. We derive thermodynamic transition levels from the formations energies for each defect in all possible charge states. In order to examine the thermodynamic stability of differently charged defect states, we calculated the formation energy according to:

$$E^{\mathrm{f}}(V_{\mathrm{X}}^{q}) = E_{\mathrm{tot}}(V_{\mathrm{X}}^{q}) - E_{\mathrm{tot}}^{\mathrm{bulk}} + \mu_{\mathrm{X}} + qE_{\mathrm{F}} + \Delta^{\mathrm{q}} \quad (1)$$

where $E_{\mathrm{tot}}(V_{\mathrm{X}}^{q})$ is the total energy of the supercell containing a vacancy of the species X in charge state q and $E_{\mathrm{tot}}^{\mathrm{bulk}}$ is the total energy of defect-free in the same supercell. The term μ_{X} is the chemical potential needed to add or remove atoms of type X to the bulk to create the defect. The Fermi level (E_{F}) is the energy of the electron reservoir in the solid. It is referenced to the valance band maximum of the STO defect-free crystal.

$$E_{\mathrm{F}} = E_{\mathrm{VBM}} + \epsilon_{\mathrm{F}} \quad (2)$$

E_{VBM} is the energy of the valence band maximum of the oxide. It can be approximated by the energy of the highest occupied KS-orbital obtained by an electronic density of states analysis of the bulk system [20]. The last term Δ^{q} denotes the Makov-Payne correction term for charged defects [21].

IV. Results

The four different defect candidates studied in this work, the oxygen vacancy $\mathrm{V_O}$, the strontium vacancy $\mathrm{V_{Sr}}$, the titanium vacancy $\mathrm{V_{Ti}}$, and the titanium antisite defect $\mathrm{Ti_{Sr}}$ are shown in Fig. 2 (top). The corresponding highest occupied molecular orbital (HOMO) is shown in Fig. 2 (bottom), demonstrating that the electronic states are localized at the defect sites. The defects were relaxed in all their possible charge states, in order to confirm the existence of a specific state, where excess charge remains localized at the defect site.

Experiments demonstrate that defects such as oxygen vacancies easily form and significantly influences both the electrical and optical characteristics of STO [22]. In STO, every oxygen atom is bonded to two Ti atoms. Therefore, forming $\mathrm{V_O}$ results in two neighboring Ti dangling bonds. The neutral charge state is located near the conduction band and occupied with two electrons with opposite spins. However, as shown in Fig. 4 (a), the neutral $\mathrm{V_O}$ is not stable for Fermi levels within the $SrTiO_3$ bandgap, making it a shallow donor with the $+2$ state being most stable. Another notable defect is the strontium vacancy. Because of the ionic nature of the bond between the Sr atoms and the $\mathrm{TiO_6}$ octahedra in

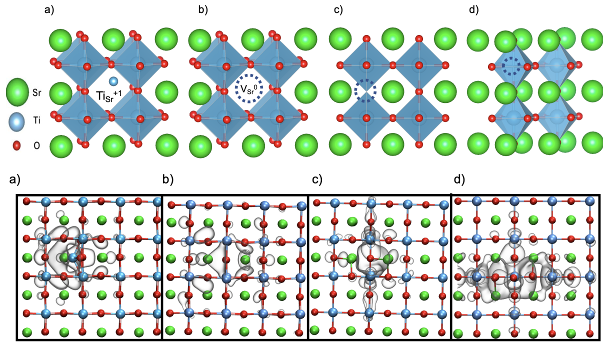

Figure 2: Top: The atomic structures of $SrTiO_3$ with a) an antisite defect Ti_{Sr} b) with a strontium vacancy V_{Sr} c) with an oxygen vacancy V_O, d) with a titanium vacancy V_{Ti}, bottom: Corresponding charge states of the same defects with their HOMO that are localized at the defect site.

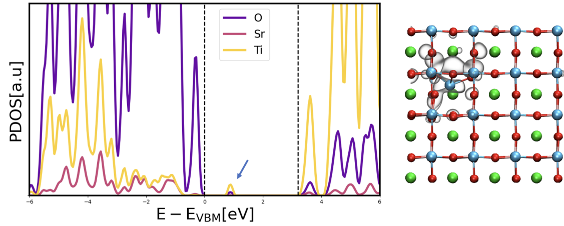

Figure 3: Projected density of states (PDOS) and localized highest occupied molecular orbitals of the titanium antisite defect.

STO, the Sr vacancy does not lead to dangling bonds. The Sr vacancy can be stabilized in the singly negative and doubly negative charge states. The formation energies of the Sr vacancy for different charge states are shown in Fig. 4 (b). The Sr vacancy is a double acceptor, with charge transition levels 0/- and -1/-2. Also, the removal of a Ti atom leads to the breaking of six Ti-O bonds, leaving six O dangling bonds and four holes. The distances between the surrounding O atoms are too large for the formation of O-O bonds. The resulting holes, instead of being uniformly distributed among all six O atoms, localize on individual O atoms. The Ti vacancy can carry charges of $q = 0, -1, -2, -3, -4$, with the formation energies shown in Fig. 4 (c).

Recent works suggest that the antisite defect Ti_{Sr}, where a Sr is replaced by a Ti atom should naturally exist [23], in particular when growing STO under Sr-deficient conditions. Ti_{Sr} is the only point defect that breaks the inversion symmetry, generating a large electric dipole. The Titanium antisite defect can carry charges of $q = 0, +1, +2$, with the formation energies shown in Fig.

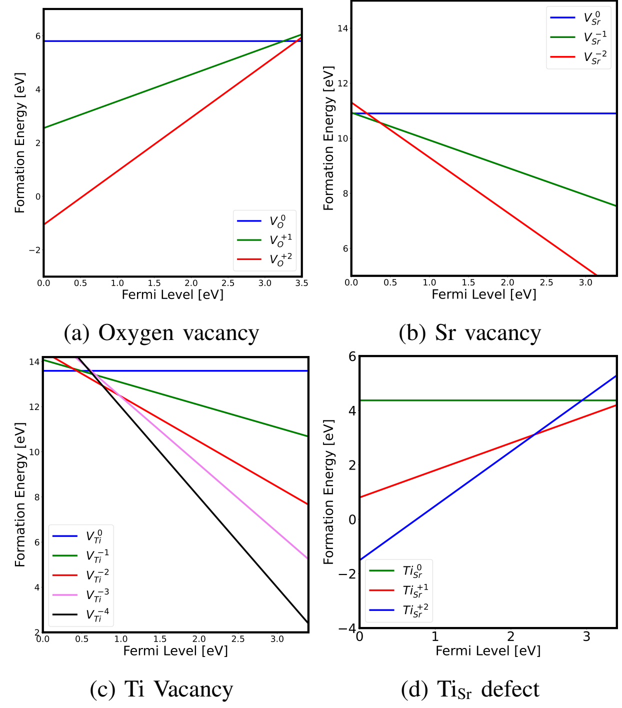

(a) Oxygen vacancy (b) Sr vacancy (c) Ti Vacancy (d) Ti_{Sr} defect

Figure 4: Formation energy as a function of the Fermi level for vacancy defects in $SrTiO_3$: (a) Oxygen vacancy, (b) Sr vacancy, (c) Ti Vacancy, and (d) Ti_{Sr} defect.

4 (d). Also, as an example Fig. 3 shows the PDOS for a singly charged antisite defect. The defect introduces localized electronic states within the $SrTiO_3$ bandgap.

The points where two stability regions intersect are referred to as thermodynamic charge transition levels (CTLs), which are equivalent to the trap level E_T in the NMP model. These CTLs, along with the rest of the NMP model parameters obtained for each specific charge transition, are summarized in Table II. Our analysis primarily concentrated on transitions involving the transfer of a single electron or hole. This focus was chosen because transitions involving multiple charges simultaneously, such as $0/+2$, typically have higher barriers [24,25]. Consequently, these transitions exhibit significantly higher relaxation energies compared to single-charge transitions. Furthermore, such many-particle processes naturally have a small capture cross section. Therefore, while a direct transition may be thermodynamically favorable, it is generally more probable for such a process to occur through multiple steps, e.g. $0 \to +1 \to +2$ instead of $0 \to +2$. To calculate the relaxation energies E_R for the transitions $0 \to +1$ and $+1 \to 0$, single point calculations were performed at $0(+1)$ on the relaxed configuration in the opposite charge state

$+1(0)$. For example, $E_R^{+1/0}$ can be calculated as the energy difference to the relaxed configuration in the new charge state:

$$E_{Relax}^{+1/0} = V^{+1}(Q_2) - V^0(Q_1) \quad (3)$$

with Q_1 and Q_2 being the equilibrium positions of the defect configuration in charge states 0 and $+1$, respectively.

Defect	Transition	E_T [eV]	ϵ_R [eV]
V_O	0/+1	3.32	0.125
	+1/+2	3.59	0.103
V_{Sr}	0/-1	-0.3	0.265
	-1/-2	0.39	0.39
V_{Ti}	0/-1	0.57	0.59
	-1/-2	0.38	0.27
	-2/-3	0.98	0.95
	-3/-4	0.54	0.55
Ti_{Sr}	0/+1	3.56	0.137
	+1/+2	2.21	1.1

Table II: Theoretical defect transition levels and parameters, as calculated with DFT. The CTLs (E_T) are given with respect to the STO valence band edge.

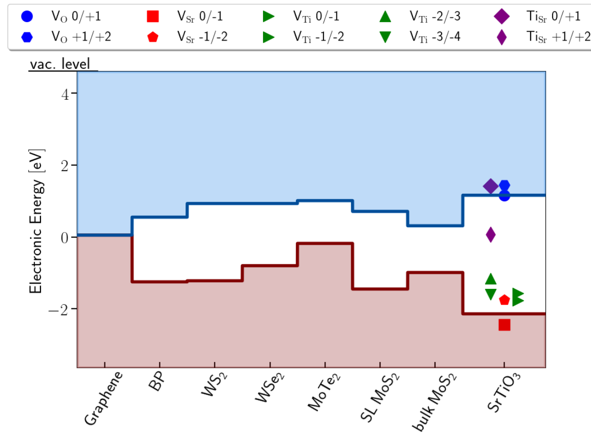

Figure 5: Trap levels of the defects within the bandgap of $SrTiO_3$ together with the band edges of commonly used 2D semiconductors in their bulk or single-layer (SL) form. V_O trap levels are shown in blue, V_{Sr} in red, V_{Ti} in green, and Ti_{Sr} in purple. The alignments of band edges and trap levels determines charge trapping and should be avoided for reliable devices [2].

The impact of charge trapping on the device reliability is predominantly influenced by the energetic alignment between the trap level of the defect and the carrier reservoirs, provided by the band edges of the semiconductor. Fig. 5 shows the calculated CTLs for four defects considered in this work together with band edges of commonly used 2D semiconductors such as MoS_2.

V. Conclusions

We investigated four different kinds of intrinsic defects in strontium titanate $SrTiO_3$ from first principles using density functional theory (DFT). These defects are expected to be relevant for the reliability of novel 2D devices. We studied the oxygen, strontium, and titanium vacancies as well as the titanium antisite defect, which can play a role for MoS_2 based devices according to its trap level. In addition, we provide defect parameters for a non-radiative multiphonon (NMP) charge trapping model, which can be used in reliability-aware TCAD simulations to improve the stability of scalable and performant 2D FETs based on STO as a high-κ gate dielectric.

References

[1] M. C. Lemme et al., *Nature Com.*, vol. 13, no. 1, p. 1392, 2022.
[2] Y. Y. Illarionov et al., *Nature Com.*, vol. 11, no. 1, p. 3385, 2020.
[3] T. Knobloch et al., *Nature Elec.*, vol. 4, p. 98–108, 2021.
[4] J.-K. Huang et al., *Nature*, vol. 605, no. 7909, pp. 262–267, 2022.
[5] A. J. Yang, et al., *Nature Elec.*, vol. 5, no. 4, pp. 233–240, 2022.
[6] G. Rzepa et al., *Microelectronics Reliability*, vol. 85, pp. 49–65, 2018.
[7] D. Waldhoer et al., *Microelectronics Reliability*, vol. 146, p. 115004, 2023.
[8] T. Grasser et al., *IEEE Trans. Electron Devices*, vol. 58, no. 11, pp. 3652–3666, 2011.
[9] K. Ralls et al., *PRL*, vol. 52, no. 3, p. 228, 1984.
[10] F. Schanovsky et al., *J. Comput. Electron.*, vol. 11, pp. 218–224, 2012.
[11] W. Goes et al., *Microelectronics Reliability*, vol. 87, pp. 286–320, 2018.
[12] T. Grasser. *Microelectronics Reliability*, vol. 52, no. 1, pp. 39–70, 2012.
[13] J. Vande Vondeleet al., *Chem. Phys.*, vol. 127, no. 11, p. 114105, 2007.
[14] T. Kühne et al., *J. Chem. Phys*, vol. 152, no. 19, p. 194103, 2020.
[15] P. Chandra et al., *Topics in Applied Physics*, vol. 105, 2007.
[16] L. Cao et al., *physica status solidi (a)*, vol. 181, no. 2, pp. 387–404, 2000.
[17] K. Van Benthem et al., *J. Appl. Phys*, vol. 90, no. 12, pp. 6156–6164, 2001.
[18] D. Gryaznov et al., *J.Phys. Chem.C.*, vol. 117, no. 27, pp. 13776–13784, 2013.
[19] R. Neville et al., *J. Appl. Phys*, vol. 43, no. 5, pp. 2124–2131, 1972.
[20] C. G. Van de Walle et al., *Journal of applied physics*, vol. 95, no. 8, pp. 3851–3879, 2004.
[21] M. Leslie et al., *J. phys.*, vol. 18, no. 5, p. 973, 1985.
[22] H. Gervasi et al., *Physical review letters*, vol. 98, no. 21, p. 216803, 2007.
[23] A. Baki et al., *Scientific Reports*, vol. 11, no. 1, p. 7497, 2021.
[24] D. Waldhoer et al., pp. 380–383, IEEE, 2022.
[25] C. Wilhelmer et al., *Microelectronics Reliability*, vol. 139, p. 114801, 2022.